# Many-body effects in bcc metals: An embedded atom model extension of the modified Johnson pair potential for iron

James R. Morris
*MS&T Division, Oak Ridge National Laboratory, Oak Ridge, Tennessee 37831-6115, USA*
*and University of Tennessee, Knoxville, Tennessee 37996-2200, USA*

Rachel S. Aga
*MS&T Division, Oak Ridge National Laboratory, Oak Ridge, Tennessee 37831-6115, USA*

Valentin Levashov
*University of Tennessee, Knoxville, Tennessee 37996, USA*

Takeshi Egami
*University of Tennessee, Knoxville, Tennessee 37996, USA*
*and MS&T Division, Oak Ridge National Laboratory, Oak Ridge, Tennessee 37831-6115, USA*
(Received 1 February 2008; published 16 May 2008)

In this work, we generalize a many-body extension of pairwise interatomic potentials originally proposed by Baskes [Phys. Rev. Lett. **83**, 2592 (1991)], in particular, showing how a pair potential interacting with multiple near neighbor shells may be extended to an embedded atom form without changing the cohesive energy or lattice constant. This is important for parametric studies of interatomic potentials, particularly how elastic constants affect other properties. Specifically, we apply this to the modified Johnson potential, a pair potential for Fe that has been used extensively for understanding liquid and amorphous metals.

DOI: 10.1103/PhysRevB.77.174201 PACS number(s): 61.50.Lt, 64.70.pe, 61.20.Ja, 62.20.dj

## I. INTRODUCTION

For many atomistic simulations, one key choice must be made as to the empirical form of the atomistic interactions.[1,2] For properties that are expected to be widely *generic*, i.e., those that may apply to a class of materials, it may be useful to choose either a simple model that does not necessarily accurately describe any particular real material. Such potentials include hard spheres, purely repulsive $1/r^n$ potentials,[3,4] or Lennard-Jones interactions.[3] On the other hand, for *material specific* properties, it is important to develop accurate potentials that capture the important energetics for the material being studied. Classical empirical potentials of interest include Stillinger-Weber interactions for Si and Ge,[5] and Tersoff[6] and Brenner[7] potentials for covalent systems including C, Si, and C-H. Empirical potentials that include electronic degrees of freedom include tight-binding models[8] and bond-order potentials;[9,10] appropriately used, these latter potentials can significantly be more accurate (although more computationally intensive) than the classical counterparts.

For metallic systems, embedded atom models[11] are many-body (MB) potentials that remedy some of the drawbacks of pair potentials while maintaining a certain simplicity and computational efficiency. In particular, the energy is expressed as a functional of pair functions, which eliminates the need for explicit three-body terms. The total energy may be written as

$$E = \sum_i \left[ F(\bar{\rho}_i) + \frac{1}{2} \sum_{j \neq i} \phi(r_{ij}) \right]. \tag{1}$$

Here, there is a pair potential $\phi(r)$ plus an embedding energy $F(\bar{\rho})$ associated with an ion embedded in a surrounding charge density $\bar{\rho}$. The density $\bar{\rho}_i$ is calculated by

$$\bar{\rho}_i = \frac{1}{\rho_0} \sum_{j \neq i} \rho(r_{ij}), \tag{2}$$

where $\rho(r)$ is the spherically symmetric electron density a distance $r$ from an atom. The parameter $\rho_0$ is defined by

$$\rho_0 = \sum_{j \neq i} \rho(r_{ij}) \tag{3}$$

in a perfect lattice at the equilibrium lattice spacing, so that for the equilibrium structure, $\bar{\rho}_i = 1$ for all atoms. This form is used in many similar potentials, including Finnis-Sinclair potentials,[12] effective medium theory,[13] and "glue" potentials.[14] Typically, these potentials are fitted to a number of parameters, including cohesive energy, surface and defect energies, and elastic constants. The parameters may be fitted to either experimental data, first-principles calculations, or a combination of these.

In certain research problems, it may be useful to choose a parametrized potential and examine the behavior as a function of the parameters. This is intermediate between the above approaches. The Lennard-Jones potential has two parameters; however, these essentially simply define the energy and length scales of the problem. In contrast, the Morse potential may be expressed in terms of natural energy and length scales, plus an additional parameter that determines the interaction range of the potential. This allows for a direct study of the effect of interaction range on the properties.

In a similar way, Baskes[15] constructed a method for systematically going from a pair potential such as Lennard-Jones to a many-body form. The interaction is constructed

 

such that, within a nearest-neighbor approximation, the cohesive energy, lattice constant, and bulk modulus are unaffected by the many-body terms. Thus, the many-body effects may be examined while keeping several important parameters fixed. Two parameters are introduced: one controls the strength of the many-body potential and one controls the range of the electron density function $\rho(r)$. By varying these parameters, a number of different lattice structures may be stabilized.

The present work generalizes the work by Baskes, in particular, extending the work beyond the nearest neighbor. This is important for considering potentials that stabilize structures other than face-centered cubic (fcc), including the body-centered cubic (bcc) phase considered here. We particularly treat the modified Johnson pair (MJ) potential for Fe,[16] which stabilizes the bcc phase over the fcc phase by having a longer ranged potential such that the second-nearest neighbors significantly contribute to the lattice stability. In effect, the six next-nearest-neighbor atoms in the bcc system are only $2(3)^{-1/2} \cong 1.15$ times as far as the eight nearest neighbors, and if the attractive interaction decays sufficiently slowly, this makes for 14 effective neighbors, compared to 12 for the fcc lattice.

The modified Johnson potential was chosen because of prior studies examining undercooled liquid and glass properties.[16] The potential is not particularly accurate for Fe, but has reasonable properties. It is also much more harmonic than the Lennard-Jones potential, which is frequently used for simulation of liquids and glasses. The Lennard-Jones potential has a Grüneisen constant of 4.5 and is too anharmonic for metals. For metallic glasses, there has been considerable interest in the effect of the Poisson ratio on the properties of glasses, including their fragility[17] and their ductility.[18] For an isotropic material, such as a glass, the Poisson ratio may be defined in terms of the bulk modulus $K$ and the shear modulus $G$:

$$\nu = \frac{3K - 2G}{2(3K + G)} = \frac{3 - 2(G/K)}{2[3 + (G/K)]}. \tag{4}$$

Thus, the Poisson ratio is directly related to the ratio $G/K$. Therefore, we are interested in developing a potential such that the cohesive energy, lattice parameter, and bulk modulus are fixed, so that relevant length and energy scales are invariant, while the Poisson ratio varies. The potential of Baskes[15] does precisely this, within a nearest-neighbor model. However, a straightforward extension of this to second-nearest neighbors results in a model where the bulk modulus significantly depends on the parameters.[19]

Therefore, the present work develops a model that includes second neighbors, maintains cohesive energy and lattice parameters, and minimally affects the bulk modulus. The paper is organized as follows: In Sec. II, the particular form of the potential is shown and the properties of the extension are developed. The effects of the parameters on bcc lattice properties, including elastic constants and phase competition with the fcc phase, are shown. In Sec. III, we specifically apply this to the modified Johnson potential. In particular, we examine the $T=0$ properties of the bcc and fcc lattices, including cohesive energies, lattice parameters, and elastic constants. The cohesive energies and elastic properties of quenched amorphous structures are also examined to show that the Poisson ratio of the amorphous system can be significantly tuned, from $\nu \cong 0.25$ for the original potential to $\nu \approx 0.38$ with the appropriate choice of many-body parameters.

## II. FORM AND PROPERTIES OF THE MANY-BODY EXTENSION

Following Baskes,[15] we assume that the embedding energy in Eq. (1) has the form

$$F(\bar{\rho}) = \frac{A}{2} F_0 \bar{\rho}[\ln \bar{\rho} - 1]. \tag{5}$$

The parameter $A$ determines the strength of the many-body potential; in the limit that $A=0$, the system will reduce to a pair potential. Note that Eq. (5) differs from the Baskes equation, in that we have a parameter $F_0$ that remains to be determined, instead of the number of nearest neighbors $Z_0$. In Eq. (1), the pair term has the form

$$\phi(r) = \phi_{pair}(r) - \frac{2}{F_0} F(\rho(r)). \tag{6}$$

Here, $\phi_{pair}(r)$ is the original pair potential. The electron density function around an atom is chosen to have the following form:

$$\rho(r) = \exp\left[ -\beta\left( \frac{r}{r_0} - 1 \right) \right], \tag{7}$$

where $r_0$ will be determined later. In the case considered by Baskes, or any nearest-neighbor only model, the parameter $r_0$ will be equal to the nearest-neighbor distance and we recover the normalization $\rho_0 = Z_0$.

Thus, Eqs. (2), (5), and (7) above introduce five additional parameters. The parameters $A$ and $\beta$ control the strength and range of the many-body term and are the only "true" parameters, as the others are determined from these. The parameter $r_0$ will be chosen such that the many-body term does not alter the near-neighbor separation, as described below, and is therefore dependent on the value of $\beta$. Similarly, the values of $F_0$ and $\rho_0$ are also dependent on $\beta$. The value of $\rho_0$ is determined by Eq. (3).

For convenience, we rewrite the total energy in terms of a pair contribution and a many-body contribution that we will examine in detail as follows:

$$E = E_{MB} + E_{pair}. \tag{8}$$

The many-body term will vanish in the limit that $A=0$. The pair term is simply

$$E_{pair} = \frac{1}{2} \sum_i \sum_{j \neq i} \phi_{pair}(r_{ij}), \tag{9}$$

while the many-body term is

$$E_{MB} = \sum_i \left[ F(\bar{\rho}) + \frac{1}{2} \sum_{j \neq i} \psi(r_{ij}) \right]. \tag{10}$$

We have introduced the notation

$$\psi(r) = -\frac{2}{F_0}F(\rho(r)). \tag{11}$$

Thus, the expression for the many-body energy also includes a pair term.

We now wish to choose the parameters $F_0$ and $r_0$ so that the equilibrium energy and lattice spacing $a_0$ do not change as the many-body potential is introduced. This implies that

$$E_{MB}(a_0) = 0 \tag{12}$$

and

$$E'_{MB}(a_0) = 0, \tag{13}$$

where $E_{MB}(a_0)$ is the energy of a perfect lattice with lattice constant $a_0$. Thus, there are two equations and two unknown quantities. Equation (12) may be satisfied if the parameter $F_0$ is defined by

$$F_0 = -\sum_{j\neq i} \rho(r)[\ln \rho(r) - 1]. \tag{14}$$

Again, in the case of a nearest-neighbor model, the parameter $F_0$ reduces to the near-neighbor coordination number $Z_0$ used by Baskes. With this choice, if the local charge density at atom $i$ is $\bar{\rho}_i = 1 + \delta\rho$, the contribution to the many-body energy in Eq. (10) is only second order in $\delta\rho$; the first-order contribution vanishes.

To satisfy Eq. (13), we must also choose a form of $\rho(r)$ that satisfies

$$\sum_{j\neq i} r_{ij} \ln \rho(r_{ij})\rho'(r) = 0. \tag{15}$$

From the form of $\rho(r)$ given in Eq. (7), we can satisfy Eq. (15) in a nearest-neighbor model simply by choosing $r_0 = 1$ (in units of the near-neighbor distance). However, for additional neighbor shells, a more general choice must be made that depends on the neighbor distribution and the parameter $\beta$. The value of $r_0$ that satisfies Eq. (15) may numerically be found in a straightforward manner.

We note that the condition for the bulk modulus to be independent of the many-body potential may be written as [analogous to Eqs. (12) and (13)]

$$E''_{MB}(a_0) = 0. \tag{16}$$

Again, for near-neighbor models, this is immediately satisfied by the above choices for $F_0$ in Eq. (14) and by choosing $r_0 = 1$ (in units of the near-neighbor distance). However, for multiple neighbors, it is not generally possible to choose a value of $r_0$ that satisfies both Eqs. (15) and (16).

### A. Example: The bcc lattice

In the above analysis, we have not used anything specific to any lattice or to any number of neighbors. As indicated above, in the case of only near neighbors, we recover $F_0 = \rho_0 = Z_0$, the number of nearest neighbors, as well as $r_0 = 1$ (in units of the near-neighbor separation). These limits also apply for large values of $\beta$, where the contribution of $\rho(r)$ past the near-neighbor shell is negligible. In the case where $\beta$ is small, in which the contributions of all neighbors considered are essentially equal, the values of $F_0$ and $\rho_0$ go to the *total* number of neighbors.

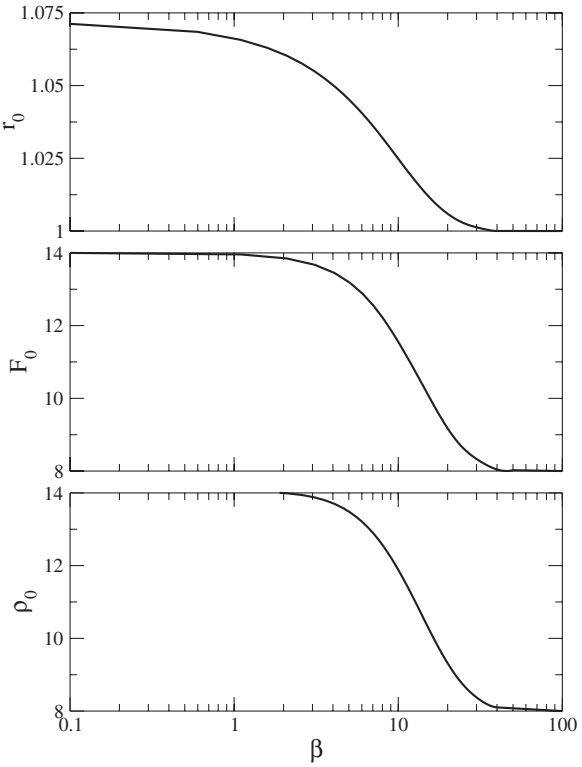


FIG. 1. Parameters $r_0$, $F_0$, and $\rho_0$ as a function of $\beta$. The parameter $r_0$ is in units of the nearest-neighbor distance; $F_0$ and $\rho_0$ are dimensionless.

To demonstrate these properties, we consider a bcc lattice and include interactions involving two neighboring shells of atoms. For a given value of $\beta$, $r_0$ is determined by numerically solving Eq. (15) (utilizing the Newton-Raphson method). We then calculate the parameters $F_0$ and $\rho_0$ by using Eqs. (3) and (14). The resulting values are shown in Fig. 1. In this figure, the value of $r_0$ is given in units of the nearest-neighbor distance. The above limiting behavior is observed: for large $\beta$, only the eight nearest neighbors contribute to $F_0$ and $\rho_0$, and Eq. (14) is satisfied with $r_0 = 1$. For small $\beta$, all 14 nearest and next-nearest neighbors contribute equally to $F_0$ and $\rho_0$. The value of $r_0$ in this limit is simply the average distance over all 14 atoms.

Note that $r_0$ does not dramatically change over the entire range of values of $\beta$. It is then tempting to replace $r_0$ by some intermediate value between the large and small limits, which is independent of $\beta$. However, such a replacement generally fails to satisfy Eqs. (12) and (13); the equilibrium lattice constant will then rapidly change as the many-body term is changed through the parameter $A$.

### B. Effect of many-body terms on the elastic constants

The many-body terms will, of course, affect the elastic constants. For a pair potential, the elasticity tensor is given by

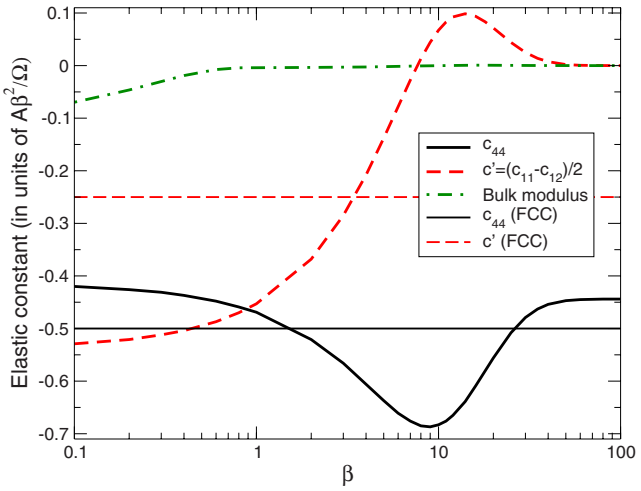


FIG. 2. (Color online) The many-body contributions to the elastic constants, as a function of the many-body term $\beta$, for a bcc lattice including second neighbors. Elastic constants are expressed in terms of the many-body terms $A$ and $\beta$, and the volume per atom $\Omega$. Lighter straight lines indicate the corresponding fcc behavior.

$$C^{\phi}_{\mu\nu,\kappa\lambda} = \frac{1}{V}\sum_{\langle ij\rangle}\left\{\frac{1}{r_{ij}^2}\left[\phi''(r) - \frac{\phi'(r)}{r}\right]x_\mu x_\nu x_\kappa x_\lambda + \frac{\phi'(r)}{r}x_\nu x_\kappa \delta_{\mu\kappa}\right\}. \tag{17}$$

In the original work by Baskes, for fcc materials, the bulk modulus $B$ and the elastic anisotropy, defined as the ratio of $c_{44}$ to $c' = \frac{1}{2}(c_{11} - c_{12})$, were shown to be independent of the many-body terms, while the many-body term contributed a term to $c_{44}$ and $c'$ given by

$$c_{44}^{MB} = 2c'^{MB} = -\frac{1}{2}\frac{A\beta^2}{\Omega}, \tag{18}$$

where $\Omega$ is the volume per atom. For any nonzero value of $A$, the elastic constants do not satisfy the Cauchy relation $c_{44} = c_{11} - c_{12}$. The fact that the bulk modulus is independent of many-body terms in the near-neighbor approximation is due to the fact that in this approximation, the many-body contribution to the energy satisfies Eq. (16) in addition to Eqs. (12) and (13) above. With the inclusion of the second-nearest-neighbor interaction, we cannot, in general, satisfy Eq. (16) as well, although we expect the effect on many-body interactions to be small.

For the bcc system, while all many-body contributions to the elastic constants scale as $-A/\Omega$, the dependency on $\beta$ is slightly different, due to the dependence of $F_0$ and $\rho_0$ on $\beta$. We show the many-body contribution to the elastic constants $c_{44}$, $c'$, and $K$ in Fig. 2, in units of $A\beta^2/\Omega$. Most importantly, the change in the bulk modulus is small for all values of $\beta$, particularly at values greater than 1. Thus, while the bulk modulus $K$ depends on the many-body potential, the effect on the two shear moduli is at least 2 orders of magnitude larger. The contribution to $c'$ is seen to vanish in the large $\beta$ limit, but is larger than for $c_{44}$ in the small $\beta$ limit.

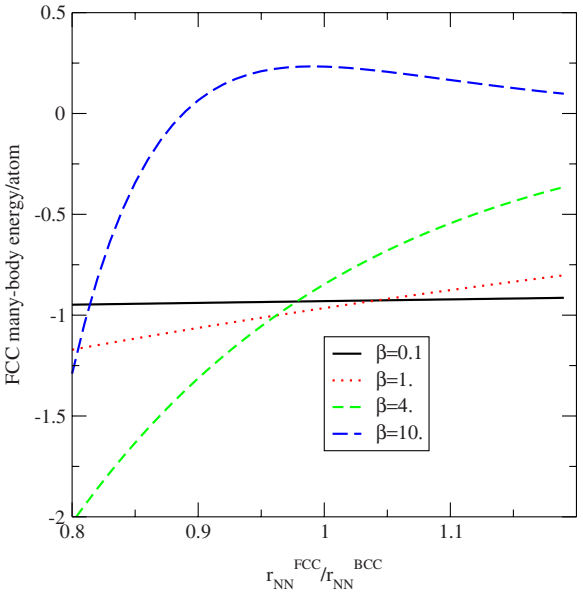


FIG. 3. (Color online) Many-body contribution to a fcc lattice, within the nearest-neighbor approximation. Energy is expressed in units of the many-body strength $A$.

### C. Effect of many-body term on fcc vs bcc phase stability

The inclusion of the many-body term will change the relative energetics of the fcc vs bcc lattice. Here, we briefly examine this. The many-body contribution to the bcc lattice energy is zero at the equilibrium lattice spacing. In Fig. 3, we show the many-body energy per atom for a fcc lattice as a function of the nearest-neighbor spacing (relative to that in the bcc lattice). We have assumed that the potential is truncated so that it includes only first-nearest neighbors in the fcc lattice. Of course, at small nearest-neighbor spacings, this assumption will break down.

For values of $\beta$ less than a critical value $\beta_c$ near 9, the many-body term adds stability to the fcc lattice, relative to the bcc lattice, with the magnitude of the difference monotonically decreasing with increasing lattice spacing. Thus, in this range, we would expect that the many-body term will both increase the fcc phase stability and decrease the nearest-neighbor spacing. The latter effect is not surprising, as the potential will try to maintain the value of $\rho_i$ close to that of the bcc lattice, despite fewer neighbors contributing. It will do so by pulling the 12 nearest neighbors closer. The value of $\beta_c$ occurs close to where $\rho_0(\beta)$ in the bcc lattice is close to the number of fcc neighbors (12), so that the total charge densities in the fcc and bcc lattices are comparable at similar near-neighbor distances. For $\beta$ near $\beta_c$, the many-body contribution to the stability of the fcc lattice is nearly zero. For larger values of $\beta$, the many-body contribution to the fcc lattice is positive, which stabilizes the bcc phase.

Note that in Fig. 3, it appears that for a given value of $\beta < 9$, the fcc lattice will prefer to go to very small spacings. This is due to the fact that we are only treating the many-body contributions; the original pair potential will presumably have a repulsive term that will stabilize the nearest-neighbor spacing close to that in the bcc lattice. Also, the results shown in Fig. 2 only include the nearest fcc neigh-

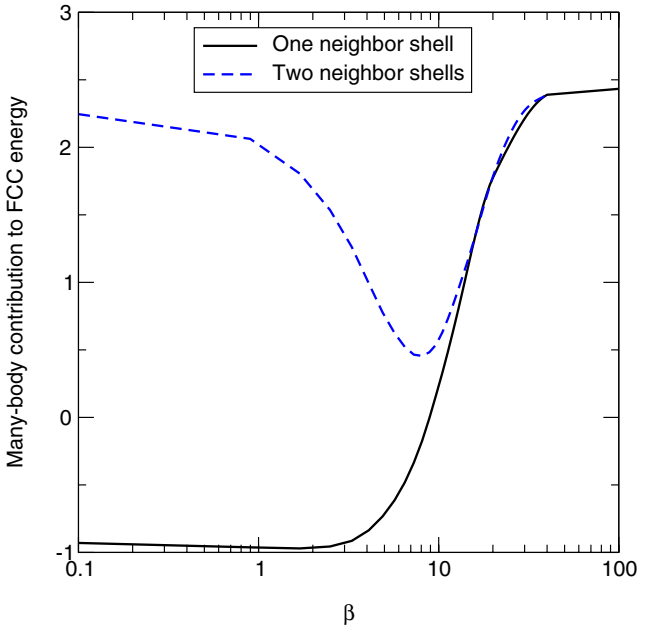


FIG. 4. (Color online) The many-body contribution to the fcc energy, assuming the nearest-neighbor distance is the same as in the bcc lattice, as a function of $\beta$, using both a nearest-neighbor approximation and a second-nearest-neighbor approximation. As in Fig. 3, the energy is in units of the many-body strength $A$.

bors, and second-nearest neighbors are excluded. If the lattice spacings were sufficiently small, then the additional neighboring shells would have to be included as well.

To demonstrate how including second-nearest neighbors affect the fcc energy, we have calculated the fcc energy by assuming the same nearest-neighbor distance as in the bcc equilibrium lattice as a function of $\beta$. Figure 4 shows this energy in the nearest-neighbor approximation and also including second-nearest neighbors. The inclusion of second-nearest neighbors makes the many-body contribution positive for all values of $\beta$, with a minimum near $\beta=\beta_c$. However, this is calculated without "relaxation"—the fcc lattice parameter is not optimized in this case. At large values of $\beta$, the curves coincide because the value of $\beta$ effectively provides a cutoff distance for $\rho(r)$. Thus, the data shown in Figs. 3 and 4 should be taken to show trends only, and unless $\beta$ exceeds $\sim$10, the competition between the bcc and fcc phases will depend on how and where $\rho(r)$ is truncated. The phase stability will have to include the truncation for the bcc and fcc lattices in a consistent manner.

## III. APPLICATION TO THE MODIFIED JOHNSON PAIR POTENTIAL

We now demonstrate the application of the above approach with a specific application. The potential we choose is the modified Johnson potential,[16] which is a simple pair potential that stabilizes the bcc phase over fcc at $T=0$. This model is chosen over Lennard-Jones because it is more harmonic and exhibits better glass forming ability. At low temperatures, the Lennard-Jones system nucleates very quickly, essentially without a barrier.[20] The Johnson potential

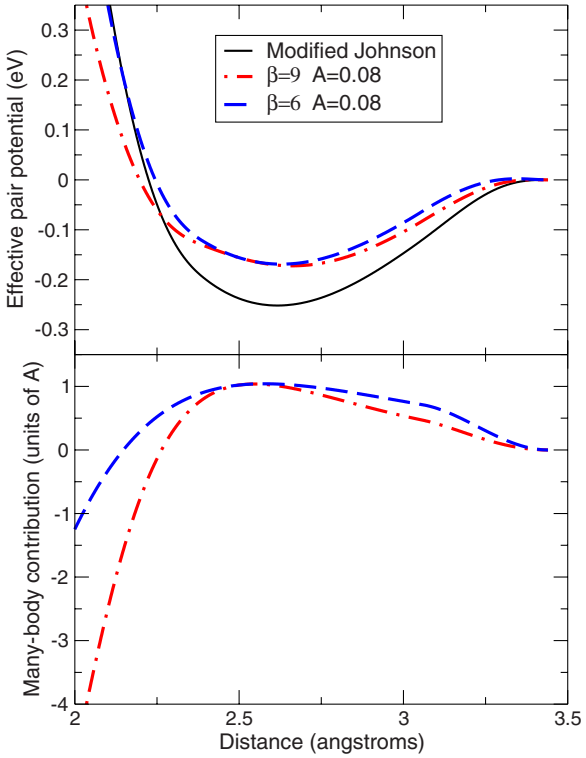


FIG. 5. (Color online) (Top) The effective pair potentials derived from the many-body contributions compared to the modified Johnson potential. (Bottom) The difference between the effective potential and the original potential, in units of the strength of the many-body parameter $A$.

is defined at interatomic distances 1.9 Å$\leq r\leq$3.44 Å as follows:

$$\phi(r)=\begin{cases}\sum_{i=0}^{4} a_i(r-2.4)^i, & 1.9\leq r\leq 2.4,\\ b_2(r-3.115\,829)^3+b_1r+b_0, & 2.4\leq r\leq 3.0,\\ \sum_{i=0}^{5} c_i(r-3.0)^i, & 3.0\leq r\leq 3.44,\end{cases} \tag{19}$$

where the constants are $a_0=-0.200\,210\,8$, $a_1=-0.504\,774\,7$, $a_2=1.372\,738$, $a_3=-15.096\,18$, $a_4=-12.900\,21$, $b_0=-1.581\,570$, $b_1=0.477\,871$, $b_3=-0.639\,230$, $c_0=-0.146\,963\,6$, $c_1=0.452\,142\,6$, $c_2=0.222\,124\,1$, $c_3=1.725\,326$, $c_4=-12.910\,63$, and $c_5=14.671\,11$. An exponential repulsive term $A_0e^{-Br}$ is added to the potential in Eq. (19) for $r\leq$1.9 Å, and the constants are $A_0=8752.934$ and $B=4.572\,488$, which are chosen to have continuous $\phi(r)$ and $\phi'(r)$ at $r=1.9$ Å. The units are such that $r$ is in Å and the energy $\phi(r)$ is in eV. A plot of the potential is shown in Fig. 5.

To make the calculations more definite and to demonstrate some of the effects of the many-body term, we also consider the above potential with additional many-body terms as described above for $\beta=6$, $\beta=9$, and $\beta=12$. We truncate $\rho(r)$

and $\psi(r)$ by multiplying these by a cutoff function as follows:

$$f_{cut}(r) = \begin{cases} 1, & r < r_n, \\ \left[1 - \left(\dfrac{r - r_n}{r_c - r_n}\right)^2\right]^2, & r_n \le r \le r_c, \\ 0, & r > r_c. \end{cases} \quad (20)$$

This form ensures that the potentials are unaltered for $r < r_n$ and go smoothly to zero at $r_c > r_n$. The derivatives are smooth at $r_n$ and $r_c$. We have chosen $r_c = 3.44$ Å to coincide with the cutoff of the Johnson potential, and $r_n = 3.0578$ Å.

It is difficult to get an intuitive feeling for the many-body potentials; however, an effective, density-dependent pair potential may be defined[21] as follows:

$$\phi_{\text{eff}}(\bar{\rho}; r) = \phi(r) + \psi(r) + 2F'(\bar{\rho})\rho(r) + F''(\bar{\rho})\rho^2(r). \quad (21)$$

This effective potential is evaluated by using the average density $\bar{\rho}$. By construction, the average density is $\bar{\rho} = 1$ in the bcc $T = 0$ phase and $F'(\bar{\rho} = 1) = 0$; therefore, the first-order term in $\rho(r)$ vanishes. The effective potentials along with the original Johnson potential are shown in Fig. 5 for three choices of the many-body potential. We have chosen $\beta = 6$, 9, and 12 for demonstration. The values of $A = 0$ and $A = 0.08$ eV were chosen to demonstrate the effect of the many-body term on the potential. The many-body effective potentials are not as deep as the original potential: near the minimum of the original potential, the many-body contribution is positive. This does not affect the cohesive energy, as there is a compensating term $F(\bar{\rho})$ that does not appear in the effective pair potential. The many-body term also softens the repulsive portion of the potential, particularly for larger values of $\beta$. For $\beta = 6$, there is a slight positive value of the effective potential near 3.3 Å. The bottom of the figure shows the contribution from the many-body addition, scaled by the strength $A$. As can be seen, this contribution to the effective potential has a value of $A$ at the near-neighbor distance and is positive but smaller for all distances greater than this. The negative curvature can create a problem if the strength of this term is too large. If $A$ is made too strong, then the many-body term dominates the original pair potential: in particular, the effective interaction will have a *negative* curvature in the region of the nearest-neighbor distance, as can be seen for $\beta = 12$, and a second local minimum in the pair potential may occur. If $A$ is sufficiently large, this minimum can be deeper than the original minimum of the pair potential. In this extreme limit, the many-body contribution is no longer a perturbative extension of the pair potential: while the original stable lattice structure is still locally stable, it may not be the true ground state of the full potential.

It is important to note that the effective potential is not a complete description; in fact, it misses several of the key properties. If an effective pair potential would suffice, then there would be no point in adding a many-body term. Some properties calculated with the effective pair potential would significantly differ from those calculated by using the full many-body potential, because the effective pair potential is defined by assuming a fixed value of $\bar{\rho}$. However, most distortions will change this value. As an example, the elastic properties calculated by using the effective pair potentials will have properties characteristic of all *pair* potentials: the Cauchy relations give $c_{44} = c_{12} = c_{11} - c_{12}$ (and, therefore, also give a Poisson ratio of 1/3). In contrast, the full many-body potential has a more complex (and realistic) behavior, as shown in Fig. 2.

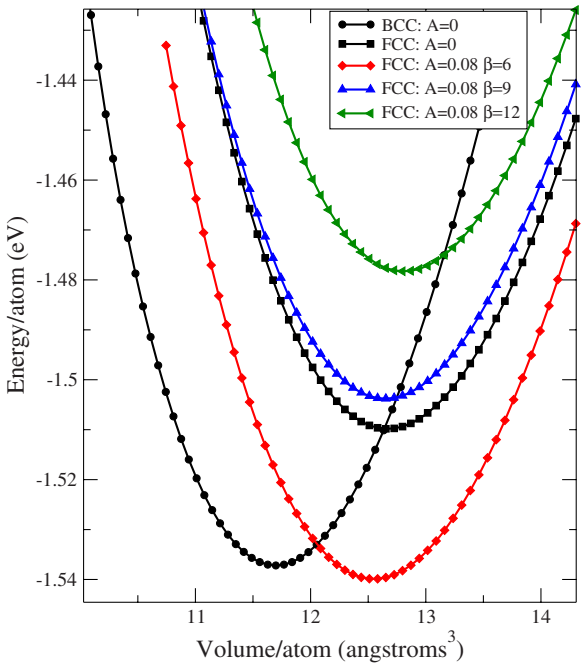


FIG. 6. (Color online) Energy vs volume for the bcc and fcc lattices, for the Johnson potential ($A = 0$) and for many-body versions with $A = 0.08$ eV and $\beta = 6$, 9, and 12. For the bcc lattice, the many-body results are indistinguishable with the $A = 0$ curve.

As indicated above, the competition between fcc and bcc phases is complex, depending on truncation. Here, we examine this in detail for the pair potential and its many-body potential. Figure 6 shows the energy vs volume for the bcc and fcc phases, for the same parameters as in Fig. 5. The bcc curves are essentially identical for all parameters, so only the value for the pair potential ($A = 0$) is shown. The fact that the minima of these curves coincide demonstrates that the cohesive energy and lattice constant are the same by construction. However, as indicated above, there is no guarantee that the curvature of these (proportional to the bulk modulus) are the same. The fact that the curves are nearly identical reflects the *near* cancellation of terms in the bulk modulus. In contrast, the fcc curves are quite distinct and reflect the trends shown in Fig. 5 for the nearest-neighbor contributions: for smaller values of $\beta$, the many-body term stabilizes the fcc phase. For larger values, the additional term favors the bcc lattice. As predicted, for $\beta = 9$, the fcc phase is nearly unchanged.

In the original work by Baskes[15] on the effects of the many-body extension of the Lennard-Jones potential, a map of the lowest energy crystal structure was shown as a function of $A$ and $\beta$. For larger values of these, structures with lower coordination numbers may be stabilized, including simple cubic and diamond cubic structures. In the present work, we also see such effects. In Fig. 7, the energies of the bcc, fcc, simple cubic, diamond cubic, and linear chain struc-

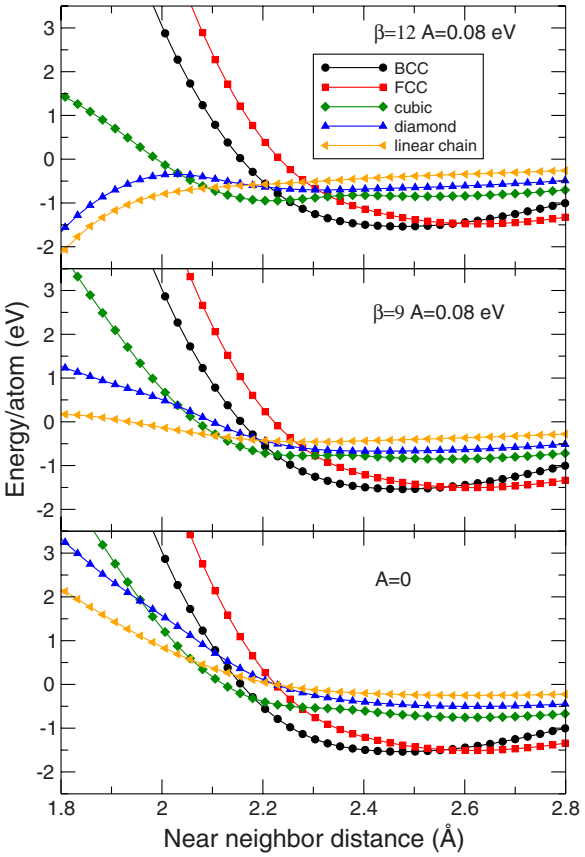


FIG. 7. (Color online) Energy vs near-neighbor distance for various crystal structures, for the Johnson potential ($A=0$) and for many-body versions with $A=0.08$ eV and $\beta=9$ and 12. As $A$ and $\beta$ are increased, the low coordination structures become more stable, which can lead to an instability at small separations.

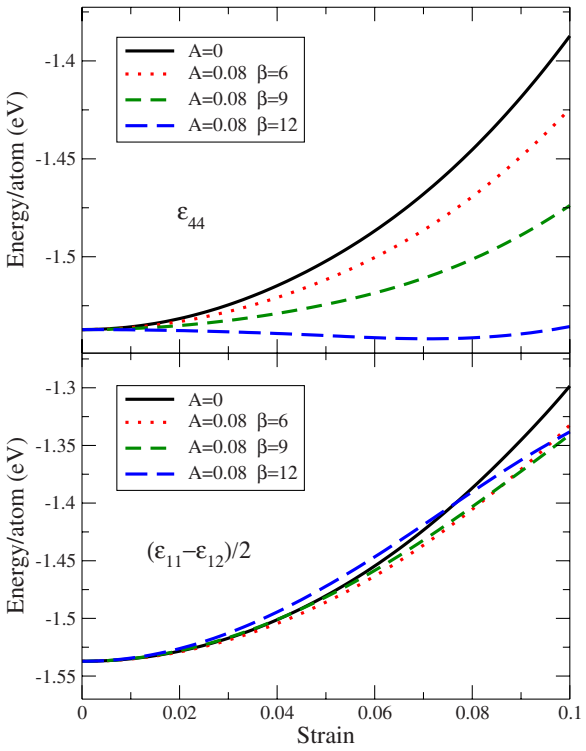


FIG. 8. (Color online) Elastic energies per atom in eV, as a function of homogeneous strain, for $A=0$ and for $A=0.08$ eV and $\beta=6$, 9, and 12.

tures are shown as a function of the near-neighbor distance, both for the original Johnson potential ($A=0$) and for $A=0.08$ eV and $\beta=9$ and 12. For $A=0$, the bcc and fcc phases are much lower in energy than the other structures. For $A=0.08$ eV and $\beta=9$, this is still the case; however, at small separations, the diamond structure and linear chain are significantly lowered in energy. In the case of $\beta=12$, there is an *instability*: the energy becomes arbitrarily low as the spacing becomes small. This is due primarily to the additional pair term given in Eq. (11). When $A$ becomes sufficiently large, this term dominates the repulsive term in the original pair potential. While there is a range of values of $A$ that stabilizes the low coordinated structures, this is due to the competition between the original potential and the additional term. The instability may be avoided either by keeping $A$ small (particularly for large $\beta$) or by strengthening the repulsion term at small distances.

### A. Elastic properties of the many-body potential

There are two distinct volume conserving strains that determine the elastic constants $C_{44}$ and $C' \equiv \frac{1}{2}(C_{11}-C_{12})$. The first may be found by considering the strain tensor[22]

$$\begin{pmatrix} 1 & \varepsilon & 0 \\ \varepsilon & 1 & 0 \\ 0 & 0 & \dfrac{1}{1-\varepsilon^2} \end{pmatrix}, \tag{22}$$

which results in a strain energy density of

$$U(\varepsilon) = 2C_{44}\varepsilon^2 + \frac{1}{4}A_4\varepsilon^4 + \frac{1}{6}A_6\varepsilon^6 + O(\varepsilon^8). \tag{23}$$

The parameters $A_4$ and $A_6$ are higher-order elastic constants beyond linear elasticity. Only even order terms appear due to the symmetry under the operation $\varepsilon \to -\varepsilon$. The energy per atom for a bcc lattice is shown in Fig. 8 for the MJ potential and for the many-body version with $A=0.08$ eV and $\beta=6$, 9, and 12, as before. A strain up to $\varepsilon=0.1$ was considered. As can be seen, there is significant softening of the lattice in the presence of the many-body term, particularly at higher values of $\beta$. For this choice of the many-body strength $A$ and this pair potential, the plot demonstrates that for sufficiently high $\beta$, the $C_{44}$ elastic constant becomes negative, which indicates a lattice instability. For $\beta=12$, there is a different minimum that develops, which indicates a transformation to a different crystal structure. (Note that the crystal phase associated with the minimum of the plot may not be stable: additional relaxations have not been allowed, so this is an upper bound to the energy of the different crystal phase.) The energies vs strain have been fitted to the form above, and the fitted values are given in Table I. The table demonstrates that both $C_{44}$ and the higher-order term $A_4$ are sensitive to the

TABLE I. Fit parameters for the distortions shown in Fig. 6 for $A=0$ and for $A=0.08$ eV and $\beta=6$, 9, and 12. The fits are to the forms given in Eqs. (23) and (25). The elastic constants (including the nonlinear terms $A_i$) are given in GPa. The many-body contribution is given in terms of the many-body terms $A$ and $\beta$, and the volume per atom $\Omega$.

| | | $\varepsilon_{44}$ strain | | |
|---|---|---|---|---|
| $\beta$ | $C_{44}$ | $A_4$ | $A_6$ | $C_{44}^{MB}$ $(A\beta^2/\Omega)$ |
| N/A | 95.2 | −23.19 | 71060 | N/A |
| 6 | 69.1 | 10.24 | 71151 | −0.66 |
| 9 | 34.2 | 74.60 | 71130 | −0.69 |
| 12 | −9.8 | 182.34 | 69872 | −0.67 |
| | | $\varepsilon'$ strain | | |
| $\beta$ | $C'$ | $A_3$ | $A_4$ | $C'^{MB}$ $(A\beta^2/\Omega)$ |
| N/A | 48.4 | 104.8 | −322 | N/A |
| 6 | 45.4 | 56.1 | −514 | −0.075 |
| 9 | 52.5 | 15.2 | −1533 | 0.046 |
| 12 | 62.1 | 77.2 | −3948 | 0.086 |

many-body term, while the term $A_6$ is essentially unchanged. Also given in the table is the contribution to $C_{44}$ that arises from the many-body term, which is in units of $A\beta^2\Omega$. The values compare well with Fig. 6.

Similarly, the value of $C'$ may be found by applying a homogeneous strain[22] as follows:

$$\begin{pmatrix} 1+\varepsilon & 0 & 0 \\ 0 & 1+\varepsilon & 0 \\ 0 & 0 & \dfrac{1}{(1+\varepsilon)^2} \end{pmatrix}. \tag{24}$$

The energy density under this homogeneous deformation is

$$U(\varepsilon) = 6C'\varepsilon^2 + \frac{1}{3}A_3\varepsilon^3 + \frac{1}{4}A_4\varepsilon^4 + O(\varepsilon^5). \tag{25}$$

The calculated energy per atom is also given in Fig. 8. Immediately, it is apparent that the many-body term affects this strain energy much less than for the $\varepsilon_{44}$ strain. No instability develops over this range of $\beta$. The fitted parameters are given in Table I. All parameters depend on $\beta$, yet the dominant term $C'$ is only weakly dependent. Again, this is consistent with the calculations in Fig. 2. By considering the entire range of $\beta$ in Fig. 2, $C'$ varies more widely than $C_{44}$; however, over the range $6 \leqslant \beta \leqslant 12$, $C_{44}$ is more sensitive. Again, the many-body contributions to $C'$ are consistent with Fig. 2.

The elastic constants for the bcc phase are summarized in Table II. The value of the bulk modulus $B$ was determined by fitting the energy vs volume shown in Fig. 6 to a fifth degree polynomial in the volume strain $\varepsilon_{vol}=(\Omega/\Omega_0)-1$, where $\Omega_0$ is the volume that minimizes the energy. Included in this table are the values of $C_{11}$, $C_{12}$, and $C_{44}$, which are all independent components of the elasticity tensor for cubic symmetry. We also express the Poisson ratio, which is given by

$$\nu = \frac{C_{12}}{C_{11}+C_{12}}, \tag{26}$$

as well as the anisotropy $(C_{44}/C')$. The Cauchy relations give $\nu=1/3$ for the pure pair potential. The table demonstrates that the dominant change is in the values of $C_{44}$ as a function of $\beta$. Thus, the anisotropy is strongly dependent on $\beta$. This is in striking contrast to the results for the nearest-neighbor fcc system, where the many-body addition does not change the elastic anisotropy.[15] The Poisson ratio exhibits nonmonotonic behavior as a function of $\beta$, but only changes by a few percent over the range of parameters considered here.

## IV. DISCUSSION

In this paper, we present a way to add a many-body term to an existing pair potential without changing the cohesive energy or lattice parameter of the reference crystal structure. This generalizes previous results that relied on a near-neighbor calculation.[15] Two additional adjustable parameters are introduced: the strength $A$ of the many-body term and a parameter $\beta$ that relates to the range of the effective charge density term $\rho(r)$. The approach is specifically demonstrated for a bcc system, including second-nearest neighbors. We demonstrate that, in general, the bulk modulus is not independent of the many-body term, unlike the nearest-neighbor version; however, for parameter ranges of particular interest, the bulk modulus is negligibly affected.

The many-body term is specifically applied to the Johnson potential, which is a pair potential that stabilizes the bcc lattice at $T=0$. For a series of parameters, the bcc energy vs volume curve is essentially unchanged: not only is the bulk modulus unchanged, but also the higher-order terms in the expansion. In contrast, the shear moduli $C_{44}$ and $C'=\frac{1}{2}$

TABLE II. Elastic constants for the bcc phase, for $A=0$ and for $A=0.08$ eV and $\beta=6$, 9, and 12. Note that for $\beta=12$, the bcc system is mechanically unstable, which results in a negative $C_{44}$ and anisotropy $C_{44}/C'$.

| $A$ | $\beta$ | $B$ (GPa) | $C'$ (GPa) | $C_{11}$ (GPa) | $C_{12}$ (GPa) | $C_{44}$ (GPa) | $\nu$ | Anisotropy |
|---|---|---|---|---|---|---|---|---|
| 0 (MJ pair) | N/A | 126 | 48.4 | 191 | 94.2 | 95.2 | 0.333 | 2.0 |
| 0.08 | 6 | 126 | 45.4 | 187 | 96.2 | 69.1 | 0.340 | 1.5 |
| 0.08 | 9 | 126 | 52.5 | 196 | 91.0 | 34.2 | 0.317 | 0.65 |
| 0.08 | 12 | 126 | 62.1 | 209 | 84.8 | −9.8 | 0.289 | −0.16 |

$(C_{11}-C_{12})$ are both changed by the many-body term. The energy vs $\varepsilon_{44}$ strain is particularly sensitive to the many-body addition; a sufficiently strong addition (and large value of $\beta$) can result in an instability. The relative stability of the fcc lattice is sensitive to the value of $\beta$ in a nonmonotonic way. The many-body term can either stabilize or destabilize the fcc lattice relative to the bcc phase.

In a subsequent paper, we will show results on disordered structures, both liquid and glass properties. These include finite-temperature properties, particularly the melting temperature of the bcc and fcc lattices, as well as the energy, structure, and elastic properties of the amorphous phases. The present results provide a basis for examining, in a systematic way, the effects of the potential on the stability of liquid and amorphous phases while preserving the $T=0$ crystal structure, density, cohesive energy, and bulk modulus.

## ACKNOWLEDGMENTS

This research has been sponsored by the Division of Materials Sciences and Engineering, Office of Basic Energy Sciences, U.S. Department of Energy under Contract No. DE-AC05-00OR-22725 with UT-Battelle. We also acknowledge computer time from the Department of Energy's National Energy Research Scientific Computing Center. J.R.M. thanks S. Namilae and W. A. Shelton for useful comments on the manuscript.

[1] A. Carlsson, Solid State Phys. **43**, 1 (1990).
[2] M. S. Daw, S. M. Foiles, and M. I. Baskes, Mater. Sci. Rep. **9**, 251 (1993).
[3] J. R. Morris and X. Y. Song, J. Chem. Phys. **116**, 9352 (2002).
[4] R. L. Davidchack and B. B. Laird, Phys. Rev. Lett. **94**, 086102 (2005).
[5] F. H. Stillinger and T. A. Weber, Phys. Rev. B **31**, 5262 (1985).
[6] J. Tersoff, Phys. Rev. B **39**, 5566 (1989).
[7] D. W. Brenner, O. A. Shenderova, J. A. Harrison, S. J. Stuart, B. Ni, and S. B. Sinnott, J. Phys.: Condens. Matter **14**, 783 (2002).
[8] C. Z. Wang and K. M. Ho, Adv. Chem. Phys. **93**, 651 (1996).
[9] A. Girshick, A. M. Bratkovsky, D. G. Pettifor, and V. Vitek, Philos. Mag. A **77**, 981 (1998).
[10] L. Goodwin, A. J. Skinner, and D. G. Pettifor, Europhys. Lett. **9**, 701 (1989).
[11] S. M. Foiles, M. I. Baskes, and M. S. Daw, Phys. Rev. B **33**, 7983 (1986).
[12] M. W. Finnis and J. E. Sinclair, Philos. Mag. A **50**, 45 (1984).
[13] K. W. Jacobsen, J. K. Norskov, and M. J. Puska, Phys. Rev. B **35**, 7423 (1987).
[14] F. Ercolessi, M. Parrinello, and E. Tosatti, Philos. Mag. A **58**, 213 (1988).
[15] M. I. Baskes, Phys. Rev. Lett. **83**, 2592 (1999).
[16] D. J. Srolovitz, K. Maeda, V. Vitek, and T. Egami, Philos. Mag. A **44**, 847 (1981).
[17] V. N. Novikov and A. P. Sokolov, Nature (London) **431**, 961 (2004).
[18] J. J. Lewandowski, W. H. Wang, and A. L. Greer, Philos. Mag. Lett. **85**, 77 (2005).
[19] S. G. Srinivasan and M. I. Baskes, Proc. R. Soc. London, Ser. A **460**, 1649 (2004).
[20] F. Trudu, D. Donadio, and M. Parrinello, Phys. Rev. Lett. **97**, 105701 (2006).
[21] S. M. Foiles, Phys. Rev. B **32**, 3409 (1985).
[22] P. Söderlind, O. Eriksson, J. M. Wills, and A. M. Boring, Phys. Rev. B **48**, 5844 (1993).